Mott-Schwinger scattering of polarized low energy neutrons up to thermal energies

M. T. Gericke,[1,*] J. D. Bowman,[2] and M. B. Johnson[3]
[1]*University of Manitoba, Winnipeg, Manitoba R3T 2N2, Canada*
[2]*Oak Ridge National Laboratory, Oak Ridge, Tennessee 37831, USA*
[3]*Los Alamos National Laboratory, Los Alamos, New Mexico 87545, USA*
(Received 17 June 2008; published 22 October 2008)

The availability of new, high-intensity, cold and thermal neutron sources has opened the possibility of performing high-precision fundamental neutron physics experiments, including measurements that study the hadronic weak interaction and standard model test measurements, using neutron β decay. The observables in these experiments are usually correlated with the direction of neutron polarization and are often very small ($10^{-8} \rightarrow 10^{-6}$). Mott-Schwinger scattering of polarized neutrons can produce spin-dependent shifts in beam centroids, which has the potential to produce significant systematic effects for these types of experiments. An accurate calculation of this process for neutral atoms and basic molecules has not been carried out for low neutron energies. In this work, we derive a general expression for the electromagnetic (Mott-Schwinger) contributions to the analyzing power for low-energy neutron scattering. We obtain numerical results for 11 nuclei in the range of $A = 1$ to $A = 208$ and provide a series of graphs for easy reference and interpolation between A values. We also estimate the contribution of spin-dependent nucleon-nucleon forces and apply our results to determine the analyzing power of parahydrogen. Numerical calculations are performed to determine the analyzing power for the parahydrogen molecule and are compared to results obtained using analytical expressions.

DOI: 10.1103/PhysRevC.78.044003 PACS number(s): 28.20.Cz, 28.20.Fc, 21.30.Cb, 24.70.+s

I. INTRODUCTION

High-precision fundamental neutron physics experiments are currently in operation or are being designed and constructed to study the interaction between hadrons and test the standard model of electroweak interactions at low energy [1–3]. These experiments often involve a beam of polarized neutrons, which is used to search for neutron spin-correlated changes in observables at the ppm to ppb level [4–6]. To observe effects at this small scale, experiments need to have excellent control of systematic effects. Spin-orbit terms in the interaction of a neutron with a molecule or atom will give rise to a shift in the beam centroid that is correlated with the neutron polarization, as a transversely polarized neutron beam traverses an experiment. Since many of the observables that are measured in these types of experiments depend on relative angles between reaction products and spatial asymmetries with respect to beam polarization, knowledge of average beam position and the size of any neutron spin correlated beam motion is crucial in the suppression of systematic effects.

For instance, the NPDGamma experiment [7–11] measures the parity-violating spatial γ-ray asymmetry from the capture of cold, polarized neutrons on the protons in a liquid hydrogen target in the reaction $\vec{n} + p \rightarrow d + \gamma$. The measured asymmetry is in the angular correlation between the neutron spin and the momentum direction of the outgoing γ ray $(\mathbf{s}_n \cdot \mathbf{k}_\gamma)$. Although knowledge of the analyzing power for neutrons scattering from molecular hydrogen is therefore important for quantifying the resulting uncertainty in NPDGamma, the importance of this effect clearly extends to any experiment performing measurements of small observables in which polarized neutrons are used. Another specific example arises in the measurement of the angular correlations in neutron β decay. The purpose of this article, which was motivated by the need to understand the systematic errors introduced by this process, is to calculate the analyzing power of neutron-parahydrogen and neutron-atom scattering theoretically and to provide a reference for experimentalists, allowing them to estimate this effect quickly, for a particular design. The article also shows that the effect vanishes for very low energy neutrons typically referred to as ultracold neutrons.

Spin-orbit terms appear in both the strong and electromagnetic interactions of polarized neutrons with parahydrogen. The general features of the electromagnetic contribution have been well-known since the classic paper of Schwinger [12], who examined the case of the scattering of an energetic neutron from a proton. The effect has also been experimentally observed [13] and is of a particular significance in neutron diffraction techniques [14] and neutron polarization [15].

To evaluate the systematic effects arising from these interactions, in the types of experiments discussed above, we have extended Schwinger's analysis to the case of a polarized neutron scattering at very low energy (in the range of zero to 25 meV) from a molecule or neutral atom, taking into account the screening due to the electron cloud.

Since the neutrons used in these experiments are of very low kinetic energy, our calculations will be done entirely in the nonrelativistic approximation. For our numerical calculations, we evaluate our expression both for scattering from the hydrogen molecule (H_2) in the para state (parahydrogen) and also for several atoms under more general conditions. Our derivations are exact for the ideal gas elements and are expected to be a good approximation for all other elements.

*Corresponding author. Tel.: +1-204-474-6203 mgericke@physics.umanitoba.ca

The remainder of this article is organized as follows. In Sec. II we first establish a set of general expressions that are valid for the description of the relationship between the analyzing power and the neutron-nucleus spin-orbit interaction, as well as for parahydrogen. We consider contributions from both the electromagnetic (Mott-Schwinger) and the strong interaction. In Sec. III we apply this analysis to the hydrogen atom and extend the predictions to larger nuclei under the approximation that these can be treated as noninteracting. In this section we make use of the fact that the strong spin-orbit force is negligible for an atom at low energy. Using phase-shift calculations, we show that that one obtains an expression for the analyzing power, for unscreened nuclei, which is identical to the one obtained by Schwinger [12] and others for higher energy neutrons [16–18]. This is remarkable, because the Born approximation is, strictly speaking, valid only at higher energies. However, we show that the reason for this result is due to the long range of the electromagnetic interaction.

In Sec. IV we apply the formalism to parahydrogen, now including the spin-orbit contribution arising from the strong interaction. We discuss our results in Sec. V.

II. GENERAL EQUATIONS FOR POLARIZED NEUTRON SCATTERING

We are interested in the evaluation of the analyzing power, $A(\theta)$, for the scattering of a neutral, spin 1/2 particle with incident $\vec{p}_i$ and final $\vec{p}_f$ momenta from an atom or molecule when the particle is polarized along the direction $\hat{n} = \vec{p}_f \times \vec{p}_i/|\vec{p}_f \times \vec{p}_i|$ normal to the scattering plane, as depicted in Fig. 1.

$$A = \frac{d\sigma/d\Omega_+ - d\sigma/d\Omega_-}{d\sigma/d\Omega_+ + d\sigma/d\Omega_-}. \tag{1}$$

Here, the subscripts $+$ and $-$ refer to the sign of the product $\vec{s}\cdot\hat{n} = \cos(\alpha)$, with $\vec{s}$ being the spin of the incident particle.

In our case, we may consider both the atom and the hydrogen molecule to be spinless for the purpose of calculating the transverse asymmetry. This is correct for parahydrogen since the two protons of the molecule are in a spin singlet state. It can be done for $(J \neq 0)$ atoms bearing in mind that at the low incident neutron energies considered here the spin-orbit component of the strong interaction contributes mostly in P waves, where the phase shifts vanish as k^3 and are therefore negligible in comparison to the Mott-Schwinger effect. It should be noted, however, that substantially larger orbital angular momenta are involved for parahydrogen, since the scattering takes place coherently from both protons, and therefore the contribution of the strong spin-orbit force is much larger.

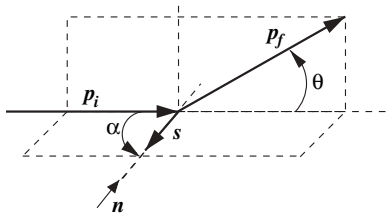

FIG. 1. Scattering diagram for Mott-Schwinger scattering of polarized neutrons. The effect vanishes for longitudinal polarization $(\vec{s})$.

For a spinless target, the asymmetry in Eq. (1) is conventionally expressed in terms of the coherent $g(\theta)$ and incoherent $h(\theta)$ scattering amplitudes which related to the S matrix as [19]

$$S = g(\theta) + ih(\theta)\vec{s}\cdot\hat{n}, \tag{2}$$

In terms of the S matrix, the differential cross section is given by

$$\frac{d\sigma}{d\Omega}_{\pm} = \chi_{\pm}^{\dagger} S^{\dagger} S \chi_{\pm}. \tag{3}$$

Where $\chi_{\pm}$ is the wave function defining the spin state of the incident neutron. The analyzing power may then be written in terms of the usual scattering amplitudes [20],

$$A(\theta) = \frac{-2\mathrm{Im}[g(\theta)h^*(\theta)]}{|g(\theta)|^2 + |h(\theta)|^2}. \tag{4}$$

$$g(\theta) = \frac{1}{2ik}\Sigma_{j\ell}(2j+1)(e^{2i\delta_{j\ell}} - 1)P_\ell(\cos\theta) \tag{5}$$

$$h(\theta) = -\frac{\sin\theta}{ik}\Sigma_\ell(e^{2i\delta_{\ell+}} - e^{2i\delta_{\ell-}})\frac{d}{d(\cos\theta)}P_\ell(\cos\theta). \tag{6}$$

Where $\delta_{j\ell}$ is the phase shift for a neutron with total angular momentum j and orbital angular momentum ℓ. $\delta_{\ell+}$ and $\delta_{\ell-}$ refer to phase shifts in states for which $j = \ell + \frac{1}{2}$ and $\ell - \frac{1}{2}$, respectively.

By expressing $A(\theta)$ in terms of the scattering phase shifts, we can relate it directly to V_{nZ} as

$$\sin\delta_{j\ell} = -\frac{2mk}{\hbar^2}\int_0^\infty r^2 dr\; j_\ell(kr)V_{nZ}^{j\ell}u_{j\ell}^{(+)}(k;r) \tag{7}$$

where $u_{j\ell}^{(+)}(k;r)$ is the outgoing solution to the Schrödinger equation, and $V_{nZ}^{j\ell}$ is the potential for a neutron in a state characterized by (j,ℓ). We begin with an exact expression for the phase shift, to avoid making any assumption about the validity of the Born approximation for this problem.

The dynamics for neutron-atom (nZ) scattering is determined by the interaction Hamiltonian $V_{nZ} = V_s + H'$, where V_s, represents the strong interaction acting between the incident neutron and the target nucleus, and

$$H' = -\vec{\mu}\cdot\vec{B}, \tag{8}$$

is the electromagnetic energy arising from the coupling between the magnetic moment $\vec{\mu} = g\mu_N\vec{\sigma}$ of the neutron and the magnetic field $\vec{B} = \vec{E}\times\vec{v}/c^2$ it experiences in its rest frame as it moves in the electric field of the atom, with relative velocity v. Here, $g = -1.91316$ is the reduced neutron gyromagnetic ratio and $\mu_N = e\hbar/2M_p$.

Because the electric field is given in terms of the Coulomb potential of the scatterer V_e by $E = -\nabla V_e$, H' in Eq. (8) may be expressed as

$$H' = -\frac{1}{m}V(r)\vec{L}\cdot\vec{s}. \tag{9}$$

Where

$$V(r) = -\frac{b}{er}\frac{\partial V_e}{\partial r} \equiv -\frac{1}{r}\frac{\partial V_b}{\partial r}, \tag{10}$$

$b = g\alpha\hbar c/Mc^2$, $V_b(r)$ is the electromagnetic potential with b replacing the charge e, m is the reduced mass of the neutron-nucleus system, and $L = \vec{r} \times \vec{p}$ is the orbital angular momentum of the neutron. For the hydrogen atom, $b \simeq -0.002933$ fm, and for the parahydrogen molecule b is smaller by about 2/3. It is assumed throughout that the potentials are spherically symmetric.

It is clear from Eq. (6) that, for scattering, any term in the interaction between the incident neutron and the target that gives rise to a difference in the partial waves $(j, \ell) = (\ell + \frac{1}{2}, j)$ and $(\ell - \frac{1}{2}, j)$ will produce a nonvanishing analyzing power. Generally, this requires a spin-dependent interaction, and the prototypical term is the spin-orbit interaction such as that given in Eq. (9). With this in mind, we may approximate Eq. (7) by

$$\sin\delta_{j\ell} = \sin\delta_{j\ell}^{(NN)} - \frac{2mk}{\hbar^2}\int_0^\infty r^2 dr j_\ell(kr)\delta V_{nH}^{j\ell} u_{j\ell}^{(+)}(k;r) \tag{11}$$

where $\delta_{j\ell}^{(NN)}$ is the phase shift for a neutron scattering due to the strong interaction V_s and $V_{nZ}^{j\ell}$ is the contribution of H' in the state characterized by (j, ℓ),

$$\delta V_{nZ}^{j\ell} \equiv \langle j\ell|H'|j\ell\rangle = -\frac{1}{m}V(r)\chi(j,l), \tag{12}$$

where

$$\chi(j,l) \equiv \begin{pmatrix} \ell, & j = \ell+ \\ -(\ell+1), & j = \ell- \end{pmatrix}. \tag{13}$$

To obtain the first term in Eq. (11) we have replaced $u_{j\ell}^{(+)}(k;r)$ by $u_{j\ell NN}^{(+)}(k;r)$, the solution to the Schrödinger equation *without* H'. Since H' is small compared to V_s, this is a reasonable approximation.

Equation (11) is the general expression we will use to calculate the analyzing power for a neutron scattering from neutral atoms (Sec. III) and parahydrogen (Sec. IV). Because we are ignoring the spin-dependent part of the strong interaction for atoms, we take the form of the interaction to be

$$V_{nZ}^{j\ell} = V_s^{(0)} + V^{(1)}\begin{pmatrix} \ell, & j = \ell+ \\ -(\ell+1), & j = \ell- \end{pmatrix} \tag{14}$$

with the strong interaction potential *without the spin-dependent terms* $[V_s^{(0)}]$ and $V^{(1)} = V_{\rm em}^{(1)} \equiv -\frac{1}{m}V(r)$ given by Eq. (9). This allows us to focus on $A(\theta)$ arising from Mott-Schwinger effects. Although Schwinger discussed the electromagnetic effect earlier, he considered only the case of a neutron scattering from a proton. For the purposes of this study, we will need to generalize this and consider neutron scattering from electrically neutral systems.

A. Electromagnetic interaction formulas

It is instructive to consider the solution to the Schrödinger equation in the WKB approximation, where we observe, at the low energies of interest in this work, that the classical turning point $r_{\rm class}$ is well beyond the range r_s of the nuclear force, $r_s \approx 1.4$ fm. We can confirm this for a 15 meV neutron noting that $r_{\rm class} \approx [\ell(\ell+1)]^{1/2}\lambda$, where $\lambda = \hbar/(2mE)^{1/2}$. For $\ell = 1$, $r_{\rm class} \approx 5.25 \times 10^4$ fm $= 0.53$Å. Because the region for $r < r_{\rm class}$ is classically excluded, and $2V(r) \ll \ell(\ell+1)/r^2$ for $r > r_{\rm class}$, these observations suggest that the centrifugal barrier dominates the interactions and we can safely replace

$$u_{j\ell}^{(+)}(k;r) \to j_\ell(kr), \quad \ell > 0 \tag{15}$$

in Eq. (11). Although the neutron can penetrate into the region $r < r_{\rm class}$ quantum mechanically, there is actually very little penetration into the region where $V(r)$ and $V_s(r)$ are appreciable (except for $\ell = 0$). The replacement in Eq. (15) is actually valid even at higher energies as well for $\ell > 0$, because the centrifugal barrier dominates the electromagnetic interaction for essentially all $r > r_s$.

The fact that the substitution in Eq. (15) is justified for $\ell > 0$ makes it possible to find a simple, general expression for $h(\theta)$ defined in Eq. (6), because S waves do not contribute here. Making use of the fact that $\delta_{j\ell}$ is small at the low energies we are considering, we may write the electromagnetic contribution Eq. (6) as

$$h^{\rm em}(\theta) = -\frac{2\sin\theta}{k}\Sigma_\ell(\delta_{\ell+} - \delta_{\ell-})\frac{d}{d(\cos\theta)}P_\ell(\cos\theta). \tag{16}$$

Now, making use of Eqs. (11), (12), and (15) , we find that Eq. (16) becomes

$$h^{\rm em}(\theta) = 4\frac{d}{d\theta}\Sigma_\ell(2\ell+1)\int_0^\infty r^2 dr\, j_\ell^2(kr)V(r)P_\ell(\cos\theta). \tag{17}$$

Assuming $V(r)$ is spherically symmetric, and making use of the partial wave expansion of a plane wave, we may write

$$\begin{aligned}\tilde{G}(q) &\equiv 4\pi\,\Sigma_{\ell>0}(2\ell+1)\int_0^\infty r^2 dr j_\ell^2(kr)V(r)P_\ell(\cos\theta) \\ &= 4\pi\int_0^\infty r^2 dr\, V(r)\big[j_0(qr) - j_0^2(kr)\big],\end{aligned} \tag{18}$$

where $q = 2k\sin(\theta/2)$ is the momentum transfer. Using the definition Eq. (10), integrating by parts, Eq. (17) becomes

$$\begin{aligned}h^{\rm em}(\theta) &= 4\int_0^\infty r^2 dr\, V(r)\frac{d}{d\theta}j_0(qr) \\ &= -2\cot(\theta/2)\int_0^\infty dx\,\sin(x)\frac{x}{q}V_b(x/q).\end{aligned} \tag{19}$$

Alternatively, is useful to note that $h^{\rm em}(\theta)$ can be expressed directly in terms of the charge density. To see how this goes, we convert the derivative with respect to θ in Eq. (19) to a derivative with respect to r and use Eq. (10)

$$h^{\rm em}(\theta) = -2\cot(\theta/2)\int_0^\infty r^2 dr\frac{dV_b(r)}{dr}\frac{d}{dr}j_0(qr). \tag{20}$$

Now, integrating by parts, we obtain

$$h^{\rm em}(\theta) = 2\cot(\theta/2)\left[r^2\,\frac{dV_b(r)}{dr}\,j_0(qr)\right]\Bigg|_{r=0} + 2\cot(\theta/2)\int_0^\infty r^2 j_0(qr)dr\left[\frac{1}{r^2}\frac{d}{dr}r^2\frac{dV_b(r)}{dr}\right]. \quad (21)$$

Using Poisson's equation, $\nabla^2 V_e = -4\pi\rho_e(r)$, Eq. (21) becomes

$$h^{\rm em}(\theta) = 2\cot(\theta/2)\left[r^2\,\frac{dV_b(r)}{dr}\,j_0(qr)\right]\Bigg|_{r=0} - 8\pi\cot(\theta/2)\int_{0+}^\infty r^2 j_0(qr)dr\rho_b(r), \quad (22)$$

where $\rho_b(r)$ is defined as the charge density with b replacing e and where the lower limit of the integration 0^+ is meant to indicate the range of integration avoids the origin, thus implying that a point charge at the origin does not contribute to the integral (the first term in Eq. (22) takes such contributions into account). The result in Eq. (22) is actually quite general and applies to any spherically symmetric system of charge density $\rho_e(r)$.

B. Strong interaction

The strong neutron-nucleus interaction is spin dependent and $g(\theta)$ must take into account the scattering lengths for the various spin states of the n-N pair. For the scattering from hydrogen, for example, we have to add both the singlet $[a(^1S_0)]$ and triplet $[a(^3S_1)]$ scattering lengths. An additional issue with $g(\theta)$ is the fact that the inelastic channel is open. According to the optical theorem this contributes to the imaginary part of the total scattering amplitude $g(\theta) = g^{\rm st}_{\rm el}(\theta) + g^{\rm st}_{\rm in}(\theta)$. At low energy, the neutron capture effect will become relevant and the Mott-Schwinger asymmetry then arises from an interference between the elastic electromagnetic scattering with all nonelastic strong processes, incorporating reactions such as (n, n'), (n, α), (n, γ), and so on. We refer to any process in which the incident neutron is completely removed as a capture process. At the low energies we are concerned with here, the capture process dominates and we want to estimate the energy at which this contribution becomes important and also to estimate its size.

Because we are considering low energy, the only relevant contributions to $g(\theta)$ are in S waves, and we write the elastic contribution as

$$g^{\rm st}_{\rm el}(\theta) = \frac{1}{k}\big[P(S=0)\big[\delta_0\big(^1S_0\big) + i\delta_0^2\big(^1S_0\big)\big] + P(S=1)\big[\delta_0\big(^3S_1\big) + i\delta_0^2\big(^3S_1\big)\big]\big], \quad (23)$$

where $P(S)$ is the projection operator onto spin S.

The cross section for the contribution of the inelastic channel is $\sigma_{\rm in} = 4\pi a_c/k$, where a_c is the neutron capture amplitude. For neutron capture the resulting compound nucleus is bound and the cross section manifests a "$1/v$" singularity. This makes the inelastic process dominate the imaginary part of the elastic scattering amplitude at sufficiently low energy. Generally, all exothermic inelastic processes, in which the incident neutron is not removed (such as: $n + A \to n' + A + \gamma$) also have this "$1/v$" cross-section behavior, but the amplitudes for such processes are very small at the low energies considered here. We obtain from the optical theorem,

$$g^{\rm st}_{\rm in}(\theta) = ia_c P(S=0). \quad (24)$$

We will ignore the real part of $g^{\rm st}_{\rm in}(\theta)$.

1. Strong scattering from hydrogen

For this case, because the capture cross section is an electric dipole transition, the reaction is dominated by $S = 0$ n-N pairs. Averaging $g(\theta)$ over the spin of the proton of the hydrogen atom and expressing the S wave phase shifts in terms of the singlet $\delta_0 = -a(^1S_0)k$ and triplet $\delta_1 = -a(^3S_1)k$ scattering lengths, we find

$$\langle g(\theta)\rangle = -\frac{1}{4}\big[a\big(^1S_0\big) + 3a\big(^3S_1\big)\big] + \frac{i}{4}\big\{a_c + k\big[a^2\big(^1S_0\big) + 3a^2\big(^3S_1\big)\big]\big\}. \quad (25)$$

For $|g(\theta)|^2$, the two spin states contribute incoherently, giving

$$|g(\theta)|^2 = \left|\frac{\delta_0 + i\delta_0^2}{k} + ia_c\right|^2 P(S=0) + \left|\frac{\delta_1 + i\delta_1^2}{k}\right|^2 P(S=1). \quad (26)$$

Averaging over the spin of the proton of the hydrogen atom, we find

$$\langle|g(\theta)|^2\rangle = \tfrac{1}{4}\big|a\big(^1S_0\big) + ika^2\big(^1S_0\big) + ia_c\big|^2 + \tfrac{3}{4}\big|a\big(^3S_1\big) + ika^2\big(^3S_1\big)\big|^2. \quad (27)$$

The contribution of the imaginary part of the amplitude in Eq. (27) is unimportant at the low energies of interest here.

We may now calculate magnitudes by taking $a(^1S_0) = -23.7$ fm and $a(^3S_1) = 5.4$ fm. This gives

$$\langle g(\theta)\rangle(\text{fm}) = 1.87 + \frac{i}{4}(a_c + 652k) \quad (28)$$

and

$$\langle|g(\theta)|^2\rangle(\text{fm}^2) = 163. \quad (29)$$

The importance of the inelastic contribution may be estimated by asking when $a_c/4$ becomes comparable to $162k$ in Eq. (28). For atomic hydrogen, using $a_c = 9 \times 10^{-5}$ fm from the capture cross section measured for thermal neutrons [21], this happens for neutron energies of about 4×10^{-4} meV, which is small compared to cold neutron energies.

However, for the more realistic case of molecular hydrogen, the parahydrogen scattering cross section is actually significantly smaller than the one calculated above [22] and becomes comparable to the capture cross section at about 1 meV, which is in the thermal energy range. In general, the significance of the inelastic contribution will vary from one material to

TABLE I. Various targets and the relevant data used for the calculation. For ^{3}He, ^{10}B, and ^{11}B, the free scattering lengths were taken directly from measured values in Refs. [25,26]. All others were calculated from the bound scattering lengths, found in Ref. [23].

	Z	J_i^π	$^{2J_+ +1}S_{J_+}$	$^{2J_- +1}S_{J_-}$	b_c (fm)	$b_{\rm ic}$ (fm)	g_+	g_-	a_+ (fm)	a_- (fm)	a_c (fm)	Ref.
^{1}H	1	$1/2^+$	$^3S_1$	$^1S_0$	−3.74	25.263	3/4	1/4	5.423	−23.748	9.0×10^{-5}	[23]
^{3}He	1	$1/2^+$	$^3S_1$	$^1S_0$	5.74	−2.5	3/4	1/4	3.5	6.1	1.48	[23,25]
^{4}He	2	0^+	$^2S_{1/2}$		3.26	0	1	0	2.6	0	2.0×10^{-8}	[23]
^{10}B	5	3^+	$^8S_{7/2}$	$^6S_{5/2}$	−0.1	−4.7	4/7	3/7	−3.8	4.7	1.1	[23,26]
^{11}B	5	$3/2^-$	$^5S_2$	$^3S_1$	6.65	−1.3	5/8	3/8	5.1	7.6	1.5×10^{-6}	[23,26]
^{12}C	6	0^+	$^2S_{1/2}$		6.65	0	1	0	6.14	0	9.8×10^{-7}	[23]
^{20}Ne	10	0^+	$^2S_{1/2}$		4.63	0	1	0	4.4	0	1.0×10^{-5}	[23]
^{27}Al	13	$5/2^+$	$^7S_3$	$^5S_2$	3.45	0.26	7/12	5/12	3.54	3.04	6.4×10^{-5}	[23]
^{28}Si	14	0^+	$^2S_{1/2}$		4.11	0	1	0	3.97	0	4.9×10^{-5}	[23]
^{40}Ar	18	0^+	$^2S_{1/2}$		1.83	0	1	0	1.79	0	1.8×10^{-4}	[23]
^{56}Fe	26	0^+	$^2S_{1/2}$		9.94	0	1	0	9.77	0	9.0×10^{-3}	[23]
^{120}Sn	50	0^+	$^2S_{1/2}$		6.49	0	1	0	6.44	0	3.9×10^{-5}	[23]
^{208}Pb	82	0^+	$^2S_{1/2}$		9.5	0	1	0	9.45	0	1.3×10^{-7}	[23]

another, due to the varying size of the capture cross section and, therefore, the inelastic strong amplitudes are taken into account for all atomic targets considered here, as well as for the parahydrogen case. At very low energies (i.e., those relevant to ultracold neutrons) the strong inelastic amplitudes completely dominate.

In addition, because the spin-orbit effects in the strong interaction need to be considered explicitly for parahydrogen, we will take $V^{(1)} = V_{\rm em}^{(1)} + V_s^{(1)}$, where $V_s^{(1)}$ is the contribution to the spin-orbit interaction arising from the strong interaction. We therefore need to make additional calculations for the strong scattering contribution to $A(\theta)$ for parahydrogen. These calculations are described separately in Sec. IV C.

2. *Strong scattering from heavier atoms*

To calculate the contribution from the strong interaction to $\langle g(\theta)\rangle$ and $\langle |g(\theta)|^2\rangle$, we obtain the free scattering lengths (a_+, a_-) from the bound coherent (b_c) and incoherent (b_{ic}) scattering lengths [23], using the relations [24,25]

$$b_c = \frac{\alpha+1}{\alpha}(g_+a_+ + g_-a_-)$$
$$b_{\rm ic} = \frac{\alpha+1}{\alpha}\sqrt{g_+g_-}\,(a_+ - a_-),$$

and

$$g_+ = \frac{J+1}{2J+1} \quad \text{for} \quad J+\frac{1}{2}$$
$$g_- = \frac{J}{2J+1} \quad \text{for} \quad J-\frac{1}{2}.$$

where α is the nucleus-neutron mass ratio.

For $J=0$ targets with neutron-nucleus orbital angular momentum $L=0$ the incoherent bound scattering length is zero and we obtain only one free scattering length from

$$b_c = \frac{\alpha+1}{\alpha}a_+ = \frac{\alpha+1}{\alpha}a\left(^2S_{\frac{1}{2}}\right),$$

which is a doublet. A few targets with $J\neq 0$ have been evaluated, because they are often used in experiments.

III. ANALYZING POWER FOR MOTT-SCHWINGER SCATTERING

Using the theory we have developed, we calculate $A(\theta)$ in this section for scattering from the hydrogen atom and heaver atoms, and then in Sec. IV we consider parahydrogen as a special case. The Mott-Schwinger analyzing power is evaluated in this section for the targets listed in Table I, which also shows the bound coherent, incoherent, and free scattering lengths used in the numerical calculations.

A. Atomic hydrogen

We begin with the calculation for atomic hydrogen, which has a charge density given by

$$\rho_e(r) = e\delta^3(r) - e\frac{1}{\pi a_0^3}e^{-2r/a_0}, \tag{30}$$

if screening by the electrons is taken into account. Here, $a_0 = \hbar^2/m_e e^2 = 0.593\text{Å}$ is the Bohr radius.

The potential energy is then

$$V_e(r) = \int \frac{\rho_e(r')}{|\vec{r}-\vec{r}'|}d^3r' = \frac{e}{r}e^{-2r/a_0}\left(1+\frac{r}{a_0}\right), \tag{31}$$

and $V(r)$ in Eq. (10) is given by

$$V(r) = \frac{b}{a_0^2 r^3}e^{-2r/a_0}\left(a_0^2 + 2ra_0 + 2r^2\right). \tag{32}$$

1. *Without screening*

If we ignore the screening due to the electron cloud around the proton, we reduce the problem to the case considered by Schwinger [12]. In the absence of screening, $V(r) = b/r^3$, and

we may evaluate Eq. (11), using Eq. (15) to obtain

$$\delta_{j\ell} = \delta_{j\ell}^{NN} + kb \begin{pmatrix} \frac{-1}{\ell+1}, & j = \ell+ \\ \frac{1}{\ell}, & j = \ell- \end{pmatrix}, \tag{33}$$

where we have made use of the fact that at the low energies we are interested in here, the phase shifts are all quite small.

Because of the short range of the nucleon-nucleon interaction, the strong-interaction phase shifts have the dependence

$$\delta_{j,l}^{NN} = \alpha_{j,l} k^{2l+1}. \tag{34}$$

Note that, in contrast, the phase shifts arising from the electromagnetic interaction have a linear dependence on k, which reflects the relatively long-range character of this interaction.

Then, according to our assumptions for scattering from individual atoms, the function $h(\theta)$ in Eq. (19) receives contributions from the electromagnetic terms only. We find, using either Eq. (19) or (22), or making use of analytical expressions [27] for the sums over the Legendre polynomials using Eqs. (33) and (16),

$$h(\theta) \equiv h^{\mathrm{em}}(\theta) = -2b \cot(\theta/2) \tag{35}$$

From Eqs. (35), (28), and (29) we find [with k expressed in fm^{-1} and b given below Eq. (10)],

$$A(\theta) = b \cot(\theta/2) \frac{a_c + 652k}{163}. \tag{36}$$

Obviously, $|h(\theta)|^2$ in the denominator of Eq. (4) is negligible except at very small angles. However, it is always included in the numerical calculations.

The electromagnetic spin-orbit terms do not contribute to $g(\theta)$ to leading order in b, but to $O(b^2)$ we find that g^{em} has a linear dependence on k,

$$g^{\mathrm{em}}(\theta) = -2ikb^2[1 + 2 \ln \sin(\theta/2)] + O(k^2). \tag{37}$$

Equation (37) is obtained by using the same analytical expressions [27] for the sums over Legendre polynomials that appear in Eq. (5) using Eq. (33).

2. *With screening*

It should be clear that the contribution $g^{\mathrm{em}}(\theta) \ll g^{\mathrm{st}}(\theta)$, so we do not have to include form-factor effects in the evaluation for $g(\theta)$. For $h^{\mathrm{em}}(\theta)$ we find immediately from Eqs. (22), (30), and (31),

$$h^{\mathrm{em}} = -2b \cot(\theta/2)[ka_0 \sin(\theta/2)]^2 \frac{2 + [ka_0 \sin(\theta/2)]^2}{\{1 + [ka_0 \sin(\theta/2)]^2\}^2}. \tag{38}$$

The result in Eq. (35) may also be obtained as the limit of Eq. (38) taking the Bohr radius a_0 to infinity. Equation (38) is finite for large q because the charge distribution for the proton has been taken to be concentrated at the origin; for parahydrogen this is not the case, and h^{em} in that case also vanishes at large momentum transfer.

Results for the angle and energy dependence of atomic hydrogen with and without screening are shown in Fig. 2. Comparing the top and bottom panels in the figure, one sees that electron screening has a large effect on the analyzing power.

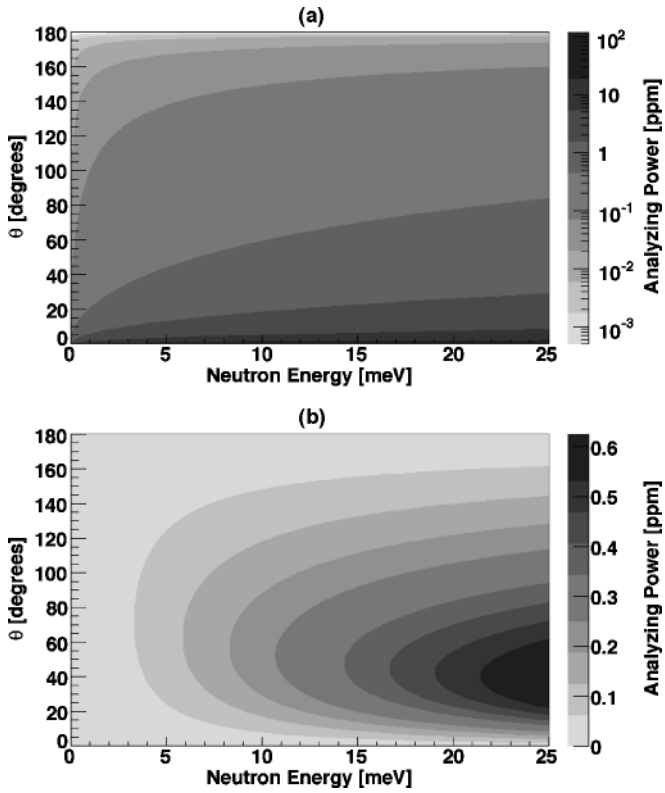

FIG. 2. Analyzing power for the unscreened hydrogen atom (a) and for hydrogen with electron screening (b). The magnitude of the analyzing power is shown. The sign of the asymmetry is negative.

B. Numerical results for larger atoms

Because of the low neutron energies involved in this study, up to 25 meV, the natural unit for momenta is the inverse of the Bohr radius a_0. The momenta of interest to cold neutron experiments are therefore $0 \leqslant ka_0 \leqslant 2.1$, and for these momenta Eq. (38) gives $h^{\mathrm{em}} \approx -b(ka_0)^2\theta$, which can be quite small at forward angles. The result is very different from the usual Mott-Schwinger result in Eq. (35) because the neutron sees the entire charge of the atom at these energies and therefore screening is maximally effective. At higher energies, though, the situation is obviously quite different.

For the electromagnetic contribution the extension to larger atoms is straightforward and achieved by substitution of $a_0 = 0.593 Z^{-1/3}$ Å in Eq. (32), which is valid assuming that the atom is in its ground ($L = 0$) state. The contributions due to the strong interaction was discussed above in Sec. (II B 2).

Numerical results for the angle and energy dependence for the analyzing power $A(\theta)$, calculated from Eqs. (4), (28), (29), (37), and (38) are shown below in Figs. 3 through 10. Naturally, we use the theory with screening included, because the atoms in experiments we envision are mostly neutral with their electron cloud completely intact.

Given that measurements of Mott-Schwinger scattering are technically difficult, we present results of extensive theoretical evaluations, which we hope will both motivate

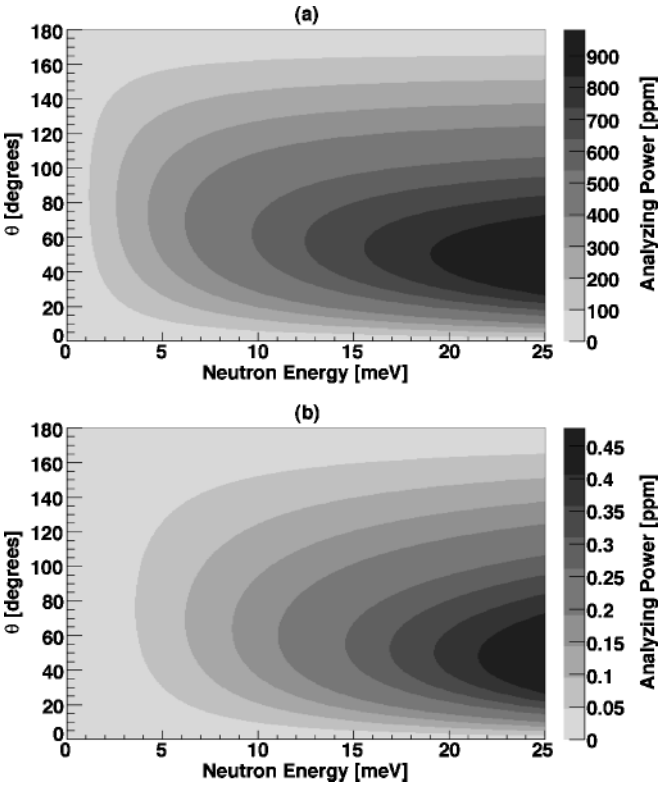

FIG. 3. Analyzing power for ^{3}He (a) and ^{4}He (b) with electron screening. The magnitude of the analyzing power is shown. The sign of the asymmetry is negative.

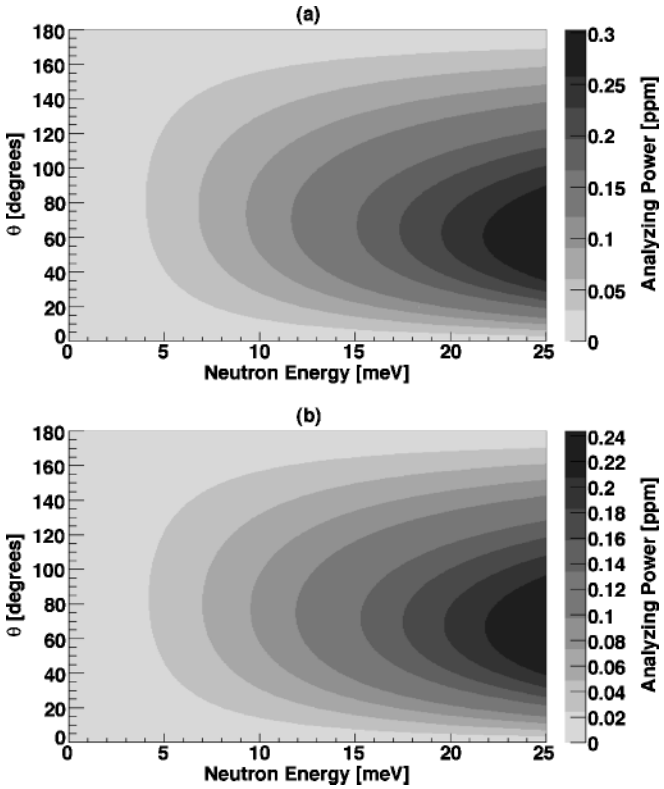

FIG. 5. Analyzing power for ^{12}C (a) and ^{20}Ne (b) with electron screening. The magnitude of the analyzing power is shown. The sign of the asymmetry is negative.

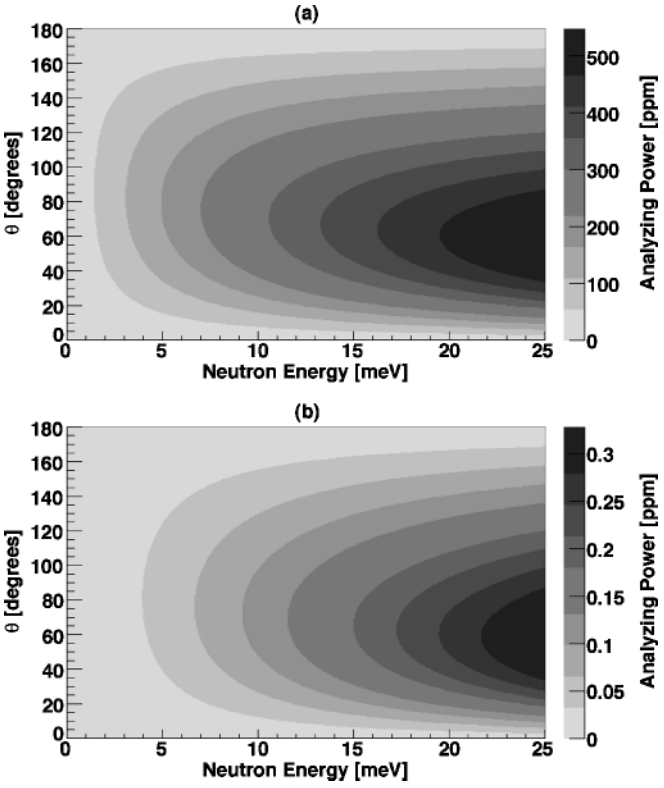

FIG. 4. Analyzing power for ^{10}B (a) and ^{11}B (b) with electron screening. The magnitude of the analyzing power is shown. The sign of the asymmetry is negative.

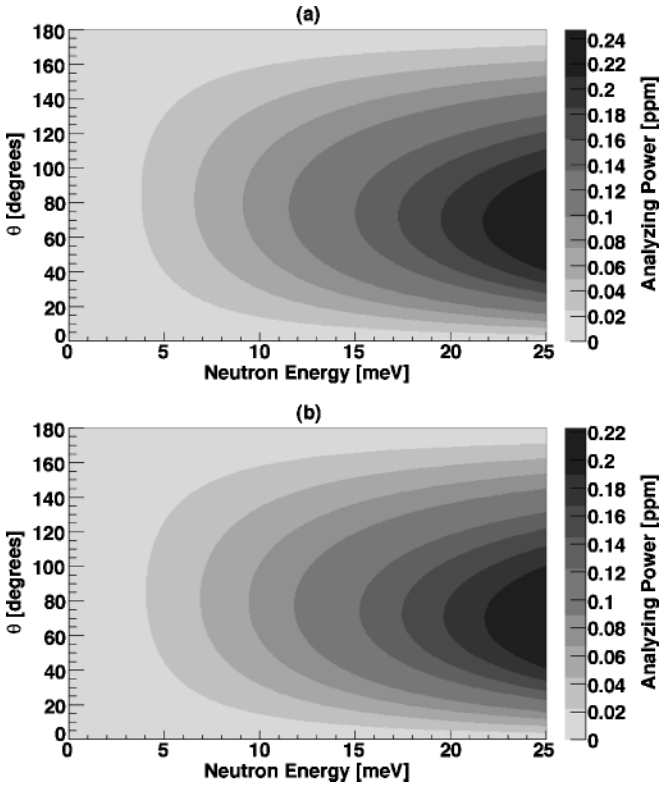

FIG. 6. Analyzing power for ^{27}Al (a) and ^{28}Si (b) with electron screening. The magnitude of the analyzing power is shown. The sign of the asymmetry is negative.

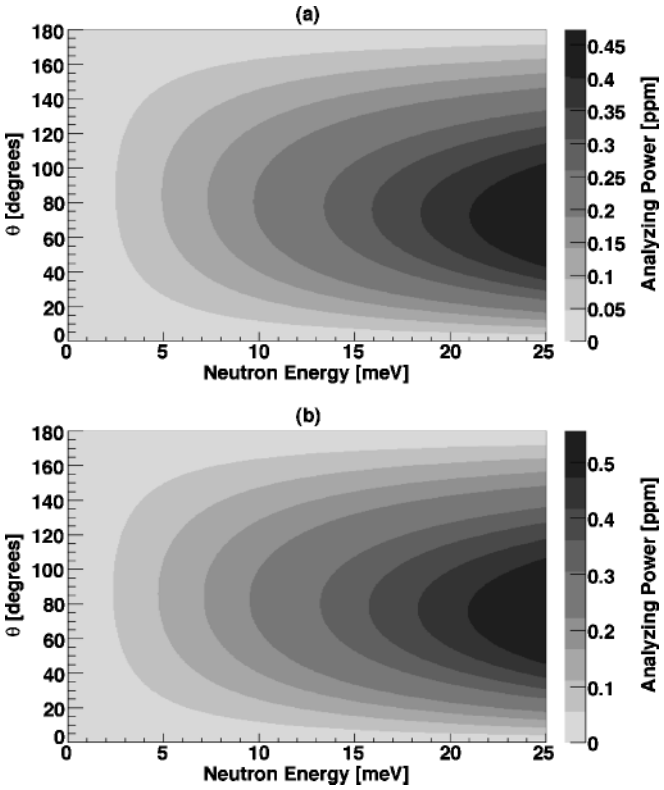

FIG. 7. Analyzing power for ^{40}Ar (a) and ^{56}Fe (b) with electron screening. The magnitude of the analyzing power is shown. The sign of the asymmetry is negative.

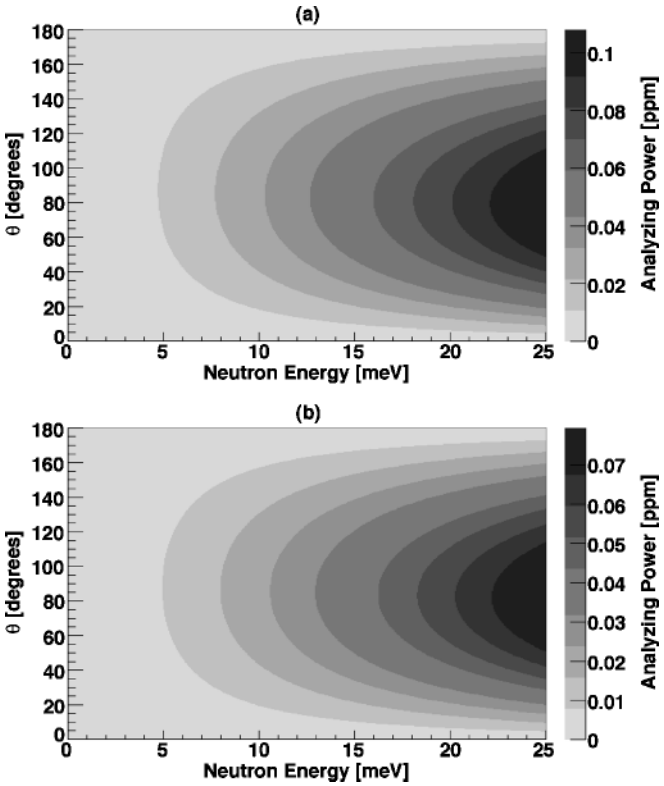

FIG. 8. Analyzing power for ^{120}Sn (a) and ^{208}Pb (b) with electron screening. The magnitude of the analyzing power is shown. The sign of the asymmetry is negative.

new measurements needed to to confirm the theory as well as facilitate extraction of relevant characteristics from the theory for evaluating systematic errors in future precision experiments. We first show, in Figs. 3–8 contour plots of the analyzing power as a function of energy and angle to give a rather complete picture of Mott-Schwinger scattering for individual atoms.

Figures 9 and 10 are provided for direct comparison of the angular and energy dependence of $A(\theta)$ for a the heavier atoms. It is clearly seen that the A dependence of the angular distributions is far from linear in A with ^{56}Fe and ^{4}He having the largest cross sections (^{10}B and ^{3}He are excluded here). The plots also show clear changes in energy and angle dependence across the mass range. The general dependence of the analyzing power on A originates in the interplay between the size of the spin-dependent interaction and the capture cross section, as seen more explicitly in Fig. 11 below. The figure shows the overall Z dependence of the analyzing power, which follows that of the electromagnetic spin-dependent scattering amplitude, with the exception of ^{40}Ar and ^{56}Fe (shown) as well as ^{10}B and ^{3}He (not shown), which have much larger analyzing powers due to their significantly larger capture cross section.

IV. ANALYZING POWER FOR A NEUTRON SCATTERING FROM PARAHYDROGEN

For parahydrogen we make the adiabatic approximation, which entails first evaluating the interactions in the body-fixed frame and then projecting into the laboratory frame by averaging over all directions of the axis of the parahydrogen molecule. Then, because the two protons of parahydrogen are in a spin singlet state, the interaction with the incident neutron in the laboratory frame will still have the form

$$V_{nH}(r,a) = V_s^{(0)}(r,a) + V^{(1)}(r,a) L \cdot \sigma_n/2, \qquad (39)$$

where the interaction $V_s^{(0)}$ is, as before, the central part of the strong interaction, and $V^{(1)} = V_{\rm em}^{(1)} + V_s^{(1)}$ now contains spin-orbit terms from both the strong and electromagnetic interactions. The spin of the protons in parahydrogen disappear from the contribution of the strong interaction $V_s^{(1)}$ when the spin average of the nucleon-nucleon spin orbit interaction is taken because the two protons are in a spin-singlet state.

In contrast to the case of the hydrogen atom, for parahydrogen the value of $h(\theta)$ now has two contributions, $h(\theta) = h^{\rm em}(\theta) + h^s(\theta)$. We examine $h^{\rm em}$ and h^s in Secs. IV B and IV C, respectively. The calculation in Sec. IV B of $h^{\rm em}(\theta)$ for parahydrogen is similar to that for atomic hydrogen, except that one uses the charge density corresponding to the parahydrogen molecule. We next turn to the derivation of this density.

A. Structure of parahydrogen

The wave function for the electrons of parahydrogen that we use is given in Ref. [28], namely

$$\phi_s(1,2) = \frac{1}{\sqrt{2(1+\Delta)}}[u(|\vec{r}_1 - \vec{a}|)u(|\vec{r}_2 + \vec{a}|) + u(|\vec{r}_2 - \vec{a}|)u(|\vec{r}_1 + \vec{a}|)]|\chi\rangle, \qquad (40)$$

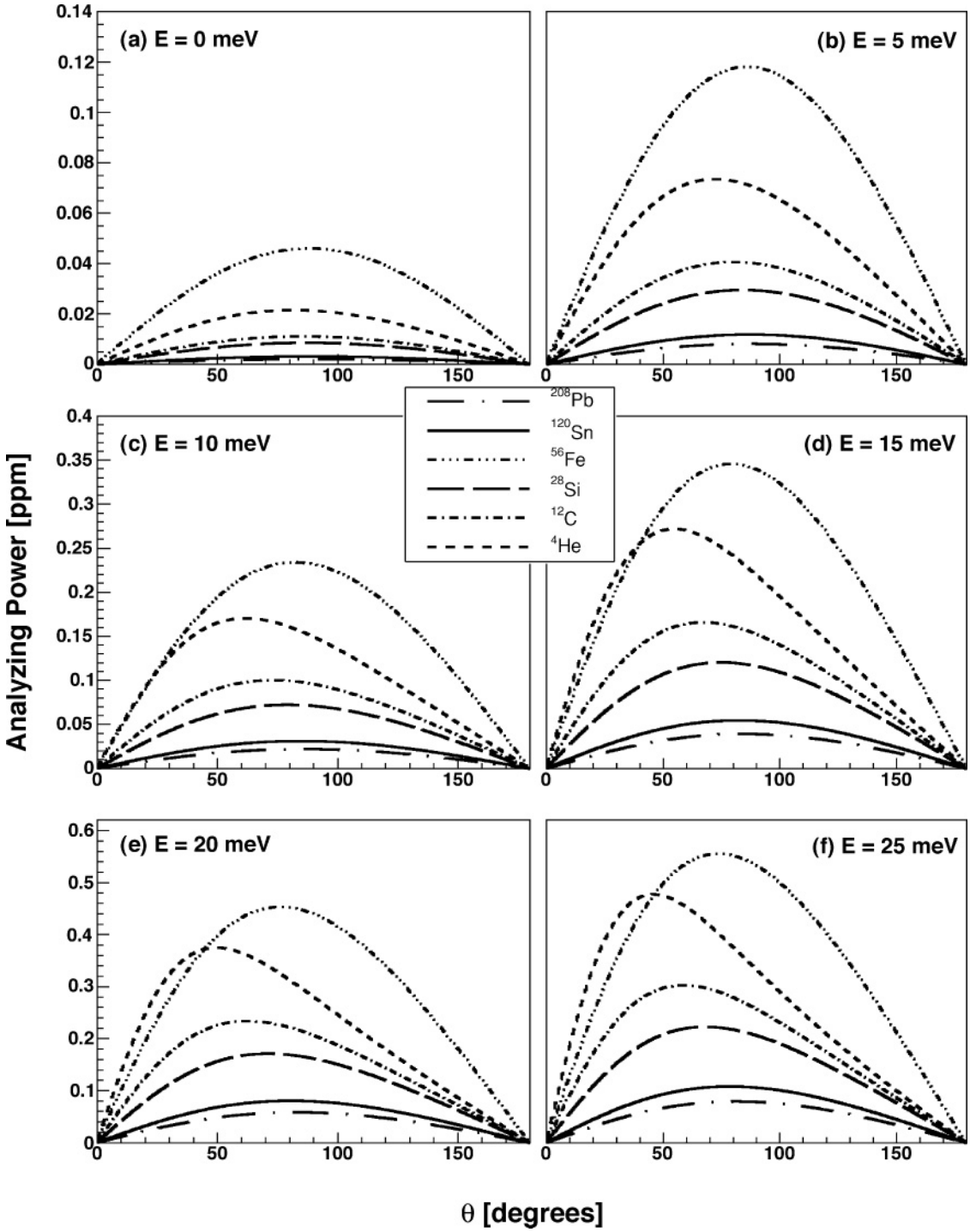

FIG. 9. Analyzing power vs. scattering angle for various targets and for energies between ≈0.1 and 25 meV, with electron screening. The magnitude of the analyzing power is shown. The sign of the asymmetry is negative.

where we have used the knowledge that the two protons of parahydrogen are in a spin singlet state,

$$|\chi\rangle = \frac{1}{\sqrt{2}}(|1/2\rangle_1|-1/2\rangle_2 - |-1/2\rangle_1|1/2\rangle_2), \quad (41)$$

so that the spatial wave function is antisymmetric under exchange of the electrons. In Eq. (40), Δ is the overlap integral,

$$\Delta \equiv \int (u(|\vec{r}_1 - \vec{a}|)u(|\vec{r}_2 + \vec{a}|))^2 d^3r. \quad (42)$$

and

$$u(r) = \frac{1}{\sqrt{\pi a_0^3}} e^{-r/a_0} \quad (43)$$

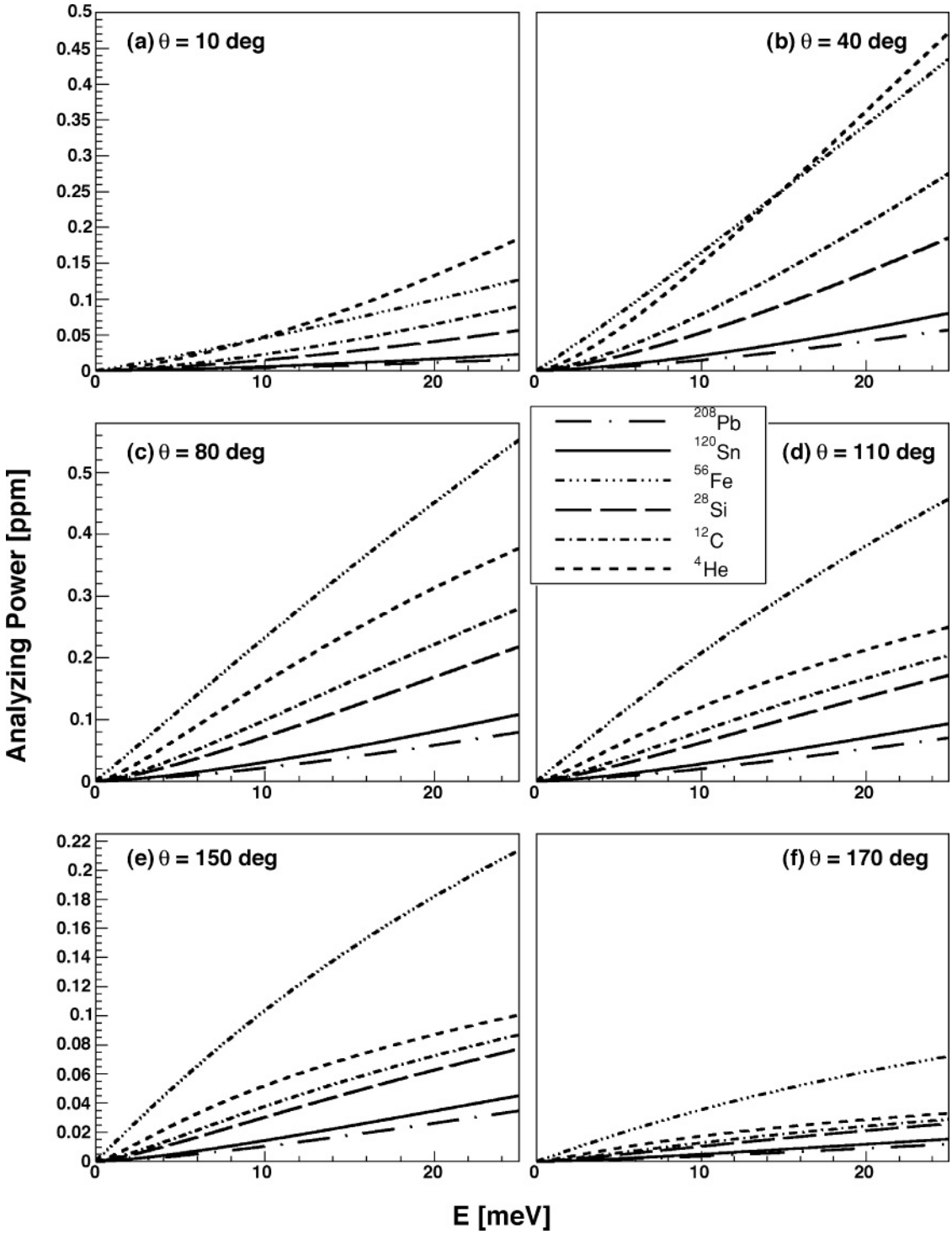

FIG. 10. Analyzing power vs. neutron energy for various targets at 10° and 20° scattering angle, with electron screening. The magnitude of the analyzing power is shown. The sign of the asymmetry is negative.

is the lowest hydrogenic electron orbit. The integral in Eq. (42) is most easily obtained analytically in prolate spherical coordinates [29]; performing the integral thus gives $\Delta \equiv \Delta(\rho) \equiv e^{-2\rho}(1+\rho+\rho^2/3)^2$ with $\rho = 2a/a_0$.

We assume the two protons are rigidly fixed a distance $2a \approx 0.74\text{Å}$ apart [29], and we place the origin of the coordinate system midway between the two protons. The charge density in the body-fixed frame is

$$\rho_e(\vec{r},\vec{a}) = e\delta^3(\vec{r}-\vec{a}) + e\delta^3(\vec{r}+\vec{a}) + \rho_e^{e^-}(\vec{r},\vec{a}), \quad (44)$$

where $\rho^{e^-}(\vec{r},\vec{a})$ is the charge density of the electrons in parahydrogen. Using the wave function in Eq. (40), we find

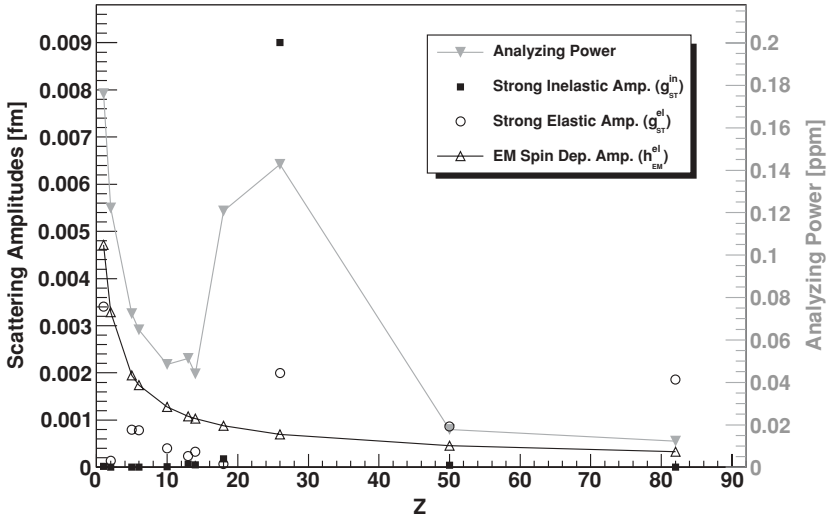

FIG. 11. Analyzing power compared to the scattering amplitudes, vs. Z for various targets at 45° scattering angle and at an energy of 9 meV. Electron screening is turned on for all targets. ^{10}B and ^{3}He are left out due to their large asymmetries, which come as a result of their large capture cross section. The elastic electromagnetic scattering amplitude is not displayed here, because it contributes only in second order and is therefore about 6 orders of magnitude smaller than the other amplitudes.

that that

$$\rho_e^{e^-}(\vec{r},\vec{a}) = \frac{e}{\pi a_0^3(1+\Delta)}(e^{-2|\vec{r}-\vec{a}|/a_0} + e^{-2|\vec{r}+\vec{a}|/a_0} + 2\Delta^{1/2}e^{-(|\vec{r}-\vec{a}|+|\vec{r}+\vec{a}|)/a_0}). \quad (45)$$

We project out the spherically symmetric component of the charge density by taking

$$\rho_e(r,a) = \int \frac{d\Omega_a}{4\pi}\rho_e(\vec{r},\vec{a}). \quad (46)$$

Using the charge density in Eq. (45), we obtain

$$\rho_e(r,a) = e\frac{\delta(r-a)}{2\pi r^2} - e\theta(r>a)\frac{\tilde{\rho}^{(1)}(r,a)}{1+\Delta} - e\theta(r<a)\frac{\tilde{\rho}^{(1)}(a,r)}{1+\Delta} - 2e\frac{\Delta^{1/2}}{1+\Delta}\rho^{(2)}(r,a), \quad (47)$$

where

$$\tilde{\rho}^{(1)}(r,a) = \frac{1}{4\pi r a a_0^2}[(2(r-a)+a_0)e^{-2(r-a)/a_0} - (2(r+a)+a_0)e^{-2(r+a)/a_0}] \quad (48)$$

and

$$\rho^{(2)}(r,a) \equiv \frac{1}{\pi a_0^3}\int \frac{d\Omega_a}{4\pi}e^{-(|\vec{r}-\vec{a}|+|\vec{r}+\vec{a}|)/a_0} \approx \frac{\Delta^{1/2}}{2\pi a^2 a_0}\frac{e^{-2\sqrt{r^2+a^2}/a_0}}{K_2(\rho)}, \quad (49)$$

where K_ℓ is a McDonald function.

Equation (49) has the following features in common with the exact $\rho^{(2)}(r,a)$: it is correct in the limit $r\to\infty$; it is very nearly correct in the limit $r\to 0$; it is correct when r is aligned along a; and it preserves the normalization of the electron density. It also has the desirable feature that with it, the contribution of Eq. (47) to $h^{\rm em}$ using Eq. (22) can be evaluated analytically. The integral and the analytical approximation are compared in Fig. 12.

B. Contribution from the electromagnetic interaction

It is instructive to examine the electromagnetic potential arising from the two protons in the laboratory frame,

$$V_e^p(r,a) = e\int\frac{d\Omega_a}{4\pi}\left(\frac{1}{|\vec{r}-\vec{a}|}+\frac{1}{|\vec{r}+\vec{a}|}\right) = \frac{2e}{r_>}. \quad (50)$$

We note that the potential corresponds to that of a charged shell of radius a, and we may make a similar observation for the parahydrogen molecule that we made earlier from consideration of the Schrödinger equation, for the hydrogen atom. Thus, also for this case, the centrifugal barrier dominates the spin-orbit interaction (at least in the absence of the strong interaction), and we can again safely make the replacement given in Eq. (15). Note that the classical turning point for $\ell = 1$, $r_{\rm class}\approx 0.64$Å, is smaller than it was for the hydrogen atom because of the larger reduced mass for the parahydrogen molecule. However, it still lies well outside the radius a of the shell of the proton charge. Thus, Eqs. (19) and (22) apply as well to parahydrogen.

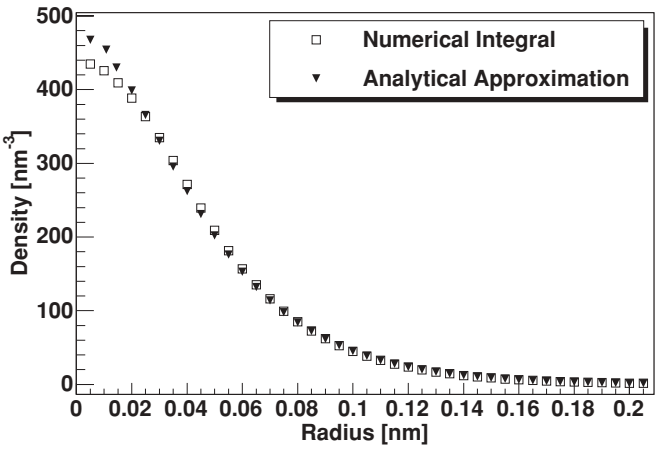

FIG. 12. Comparison between the numeric integration and an analytic approximation for part of the liquid hydrogen electron charge density.

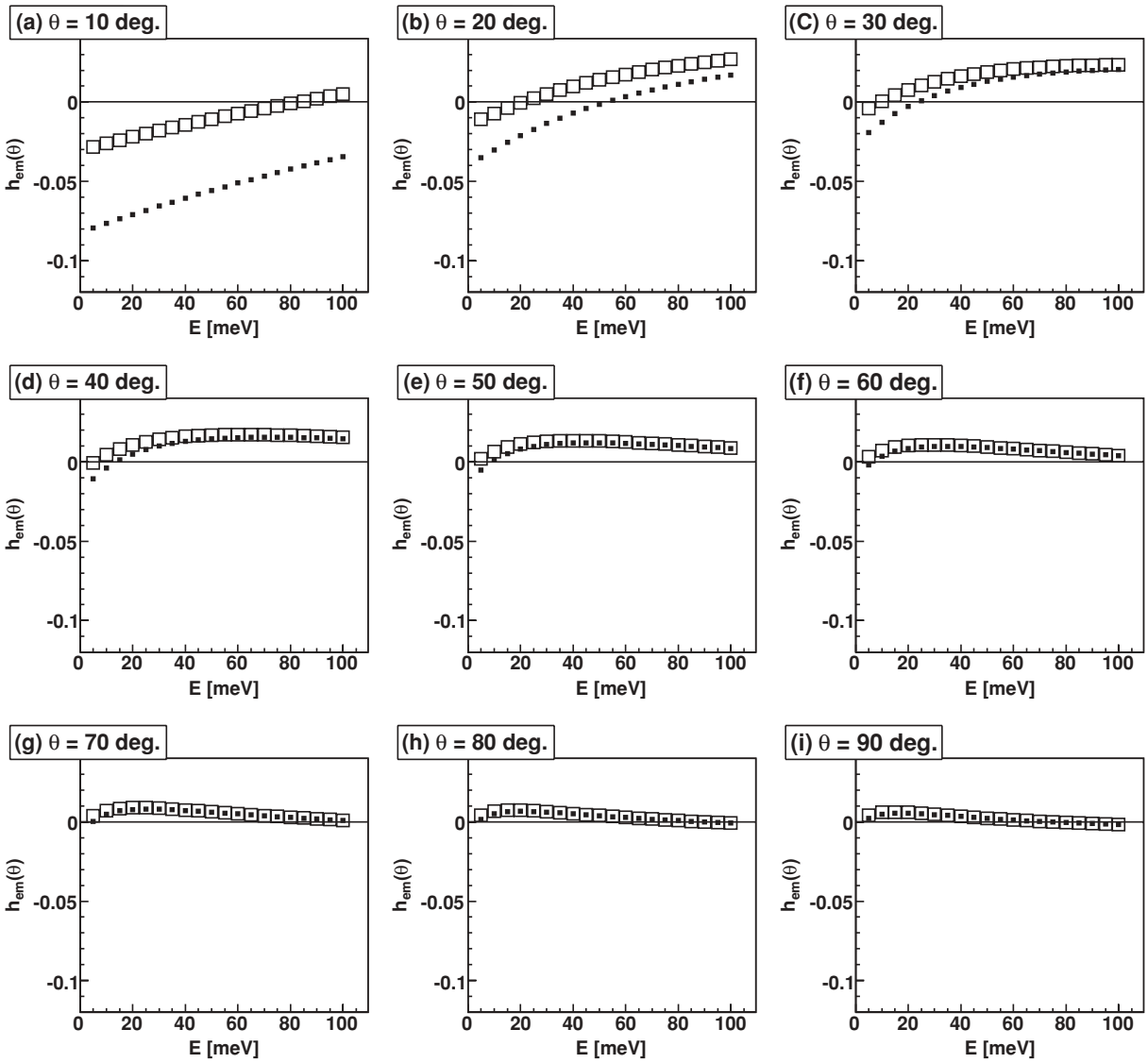

FIG. 13. Comparison of h^{em} as calculated from the analytical approximation using Eq. (49) (large open squares) and the numerical integration of Eq. (47) (small solid squares).

We find it most convenient to use Eq. (22) for the calculation. Our result for the Mott-Schwinger contribution to h^{em} for parahydrogen is thus found from

$$h^{\mathrm{em}} = -8\pi b \cot(\theta/2) \int_0^\infty r^2 \rho_b(r,a) j_0(qr) dr. \qquad (51)$$

Using Eq. (47) and Eq. (49), we find

$$\int_0^\infty r^2 \rho_b(r,a) j_0(qr) = b \frac{j_0(qa)}{2\pi} \left[1 - \frac{1}{(1+\Delta)\left(1+\frac{q^2a_0^2}{4}\right)^2} \right] - \frac{b\Delta}{1+\Delta} \frac{K_2\left(\frac{a}{a_0}\sqrt{4+q^2a_0^2}\right)}{2\pi K_2(\rho)} \frac{1}{1+\frac{q^2a_0^2}{4}}. \qquad (52)$$

Figure 13 compares the results for h^{em} obtained using the analytical approximation [Eq. (49)] and the numeric integration of Eq. (47). The two methods are almost exact for scattering angles of $\theta = 45^\circ$ or more and give reasonable agreement down to $\theta = 30^\circ$ above energies of 30 meV. Note, that h^{em} changes sign as the angle and neutron energy increases and that the analytical approximation does so at different energies and angles, as opposed to the exact value. However, for experiments using higher neutron energies or larger scattering angles, Eq. (49) provides a good approximation. Because the analytical formula is easily evaluated it provides a useful method for obtaining predictions in regions where it is valid, which can be easily determined from Fig. 13.

C. Contributions of the strong interaction

The strong interaction must be considered both for the spin-spin and spin-orbit contributions.

1. *Contribution of the strong spin-orbit force*

We assume that the spin-orbit contributions to the nucleon-nucleon phase shifts of the strong interaction can be calculated from the potential

$$V_{NN}^{\rm LS}(r) = v(r) L \cdot S, \tag{53}$$

where

$$v(r) = \lambda_{\rm LS} \frac{e^{-\mu r}}{\mu r}, \tag{54}$$

and where S is the spin of the nucleon-nucleon pair. The range, defined by $\mu = 760$ MeV/$\hbar c$, is given by the mass of the ρ meson, which is the dominant piece of the strong spin-orbit interaction. We assume that $\lambda_{\rm LS}$ has been defined so that it reproduces the spin-orbit contribution to the nucleon-nucleon phase shifts in the Born approximation,

$$\delta_{\rm JL}^{(LS)} = -\frac{2mk}{\hbar^2} \int_0^\infty r^2 dr j_L^2(kr) v(r) \langle JL|L \cdot S|JL\rangle. \tag{55}$$

where J and L are, respectively, the total angular momentum and orbital angular momentum of the nucleon-nucleon system. We find that the spin-orbit contribution to the low-energy P wave phase shifts can be reproduced by the expression

$$\delta_{\rm JL}^{\rm LS}({\rm expt}) = 0.0298\, k^3 \langle JL|L \cdot S|JL\rangle, \tag{56}$$

where k is expressed in units of fm^{-1}. We find that $\lambda_{\rm LS} = 1577$ MeV.

The quantity $V_s^{(1)}(\vec{r}, \vec{a}) \equiv < 0|[V_{NN}^{\rm LS}(|\vec{r} + \vec{a}|) + V_{NN}^{\rm LS}(|\vec{r} - \vec{a}|)]|\chi\rangle$, the spin-orbit interaction in the ground state of parahydrogen, is then

$$\frac{i}{\hbar} V_s^{(1)}(\vec{r}, \vec{a}) = (v(|\vec{r} - \vec{a}|) + v(|\vec{r} + \vec{a}|))\sigma \cdot r \times \frac{\partial}{\partial r} + [v(|\vec{r} + \vec{a}|) - v(|\vec{r} - \vec{a}|)]\sigma \cdot a \times \frac{\partial}{\partial r}. \tag{57}$$

We obtain $V_s^{(1)}(r, a)$ by averaging over the direction of $\vec{a}$,

$$V_s^{(1)}(r, a) L \cdot \frac{\sigma_n}{2} = \int \frac{\Omega_a}{4\pi} V^{(1)}(\vec{r}, \vec{a}), \tag{58}$$

finding

$$V_s^{(1)}(r, a) = -2\lambda_{\rm LS}\big[j_0(i\mu r) h_0^{(1)}(i\mu a) - 3 j_1(i\mu r) h_1^{(1)}(i\mu a)\big], \quad r < a \tag{59}$$

and

$$V_s^{(1)}(r, a) = -2\lambda_{\rm LS}\big[j_0(i\mu a) h_0^{(1)}(i\mu r) - 3 j_1(i\mu a) h_1^{(1)}(i\mu r)\big], \quad r > a. \tag{60}$$

Because the Bessel functions drop exponentially away from $r = a$, Eqs. (59) and (60) lead to

$$V_s^{(1)}(r, a) \approx -\frac{2\lambda_{\rm LS}}{(\mu r)(\mu a)} e^{-\mu|r-a|}. \tag{61}$$

Note that this potential is not small compared to the centrifugal barrier, $2m V_s^{(1)}(r, a) \gg \ell/r^2$. However, the fact that $a_0 \mu \approx 2 \times 10^5 \gg 1$ means that the spin-orbit potential is quite small (the important scale is the magnitude of the potential on the shell times the thickness of the shell), implying that the Born approximation is still valid for parahydrogen when the strong interaction is considered. The same considerations apply for the central part of the interaction. Thus, we are justified to continue using the Born approximation for our calculations.

In the Born approximation, the quantity $h^s(\theta)$ is evaluated from Eq. (61) using an expression similar to Eq. (19),

$$h^s(\theta) = -\frac{4m}{\hbar^2} \int_0^\infty r^2 dr V_s^{(1)}(r, a) \frac{d}{d\theta} j_0(qr) \approx \frac{8m\lambda_{\rm LS}}{\hbar^2 \mu^3} a \frac{d}{d\theta} j_0(qa), \tag{62}$$

Using the fact that $a_0 \gg 1$, we find that for small θ,

$$h^s(\theta) \approx 8m\lambda_{\rm LS}\left[-\frac{2(ka)(ka\theta)}{3}\right]\frac{2}{\mu^3}. \tag{63}$$

The contribution of $h^s(\theta)$ is more important for parahydrogen than it is for the hydrogen atom because of the higher angular momentum ($\ell \approx ka$) involved here.

2. *Contribution of the strong central force*

As in the case of the spin-orbit force, we assume that the contributions of the central interaction to the nucleon-nucleon phase shifts of the strong interaction can be calculated from the potential

$$V_{NN}^{(0)}(r) = v(r), \tag{64}$$

where

$$v(r) = \lambda \frac{e^{-\mu r}}{\mu r}, \tag{65}$$

and

$$\lambda = \lambda_0 P(S = 0) + \lambda_1 P(S = 1). \tag{66}$$

Although the central interaction has a strong repulsive core followed by a region of attraction, at the low energies we consider here we do not need to consider this level of detail. We take the range defined by $\mu = 760$ MeV/$\hbar c$ to be the same as for the spin-orbit force, because the core is dominated by the ω meson, which has nearly the same mass as the ρ. We assume that λ_0 and λ_1 have been defined so that they reproduce the $^1S_0$- and $^3S_0$-wave contributions to the nucleon-nucleon phase shifts in the Born approximation,

$$\delta_0 P(S = 0) + \delta_1 P(S = 1) = -\frac{2mk}{\hbar^2} \int_0^\infty r^2 dr j_0^2(kr) v(r). \tag{67}$$

The quantity $V_s^{(0)}(\vec{r}, \vec{a})$, the central component of the strong interaction in the ground state of parahydrogen, is then

$$V_s^{(0)}(\vec{r}, \vec{a}) \equiv \langle 0|\big[V_{NN}^{(0)}(|\vec{r} + \vec{a}|) + V_{NN}^{(0)}(|\vec{r} - \vec{a}|)\big]|0\rangle. \tag{68}$$

We obtain $V_s^{(0)}(r, a)$ by averaging over the direction of $\vec{a}$,

$$V_s^{(0)}(r, a) = \int \frac{d\Omega_a}{4\pi} V^{(0)}(\vec{r}, \vec{a}), \tag{69}$$

finding

$$V_s^{(0)}(r,a) = -2\frac{\lambda_0+3\lambda_1}{4} j_0(i\mu r)h_0^{(1)}(i\mu a), \quad r<a \quad (70)$$

and

$$V_s^{(0)}(r,a) = -2\frac{\lambda_0+3\lambda_1}{4} j_0(i\mu a)h_0^{(1)}(i\mu r), \quad r>a. \quad (71)$$

Because the Bessel functions drop exponentially away from $r=a$, Eqs. (70) and (71) lead to

$$V_s^{(0)}(r,a) = \frac{\lambda_0+3\lambda_1}{4}\frac{1}{(\mu a)(\mu r)}e^{-\mu|r-a|}. \quad (72)$$

Using Eqs. (5), (11), and (18), we find that $g^s(\theta)$ may be calculated from Eq. (69) using

$$\begin{aligned} g^s(\theta) &= -\frac{4m}{\hbar^2}\int_0^\infty r^2 dr\, V_s^{(0)}(r,a) j_0(qr) \\ &\approx -\frac{4m}{\hbar^2} j_0(qa)\int_0^\infty r^2 dr\, V_s^{(0)}(r,a). \end{aligned} \quad (73)$$

This may be related back to the phase shifts using Eq. (67),

$$\begin{aligned} g^s(\theta) &\approx -\frac{4m}{\hbar^2} j_0(qa)\int_0^\infty r^2 dr\, V_s^{(0)}(r,a) \\ &\approx -2\frac{a\left({}^1S_0\right)+3a\left({}^3S_1\right)}{4} j_0(qa). \end{aligned} \quad (74)$$

Comparing this to Eq. (25), we see that the scattering is the same as that from two protons but modified by the form factor arising from the fact that the protons are on a spherical shell of radius a. However, $|g^s(\theta)|^2$,

$$|g^s(\theta)|^2 = 4\left[\frac{a\left({}^1S_0\right)+3a\left({}^3S_1\right)}{4}\right]^2 j_0^2(qa), \quad (75)$$

which differs from Eq. (27) because in parahydrogen the scattering takes place coherently from the two protons. Because the scattering is purely elastic at these energies (if we ignore the capture reaction), we may get the imaginary part of $g^s(0)$ from the optical theorem,

$$\begin{aligned} Img^s(0) &= \frac{k}{4\pi}\int d\Omega |g^s(\theta)|^2 \\ &= \frac{4k}{2(ka)^2}\left[\frac{a\left({}^1S_0\right)+3a\left({}^3S_1\right)}{4}\right]^2 \int_0^{2ka}\frac{dx}{x}\sin^2(x). \end{aligned} \quad (76)$$

Alternatively, one may evaluate $g(\theta)$ from Eq. (5) expanded to second order in the phase shift of neutron-parahydrogen scattering,

$$g(\theta) = \frac{1}{k}\sum_\ell (2\ell+1)\left(\delta_\ell + i\delta_\ell^2\right)P_\ell(\cos\theta), \quad (77)$$

with

$$\begin{aligned} \delta_\ell &= -\frac{2mk}{\hbar^2}\int_0^\infty r^2 dr\, j_\ell^2(kr)V_s^{(0)}(r,a) \\ &\approx -\frac{4m}{\hbar^2} j_\ell^2(qa)\int_0^\infty r^2 dr\, V_s^{(0)}(r,a), \end{aligned} \quad (78)$$

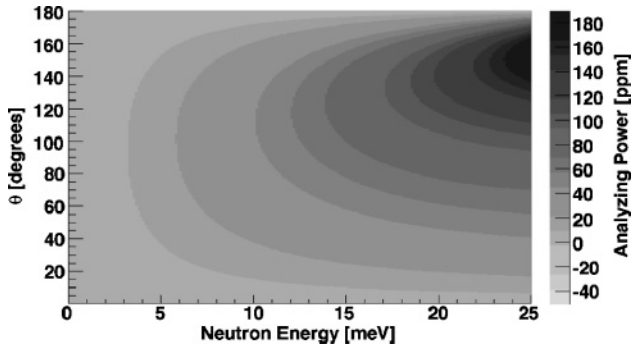

FIG. 14. Analyzing power parahydrogen, with electron screening. The magnitude of the analyzing power is shown. The sign of the asymmetry is negative.

again noting that the integral may be done analytically using the expression for $V_s^{(0)}$ in Eq. (72). The form factor is clearly going to be different for the real and imaginary parts of $g(\theta)$, and the sum over ℓ for the imaginary part will require a straightforward numerical evaluation.

3. *Numerical results*

We may obtain the analyzing power for parahydrogen using Eq. (4) from Eqs. (76), (75), (63), (51), and (53). The results are shown in Figs. 14 and 15. Note that the analyzing power

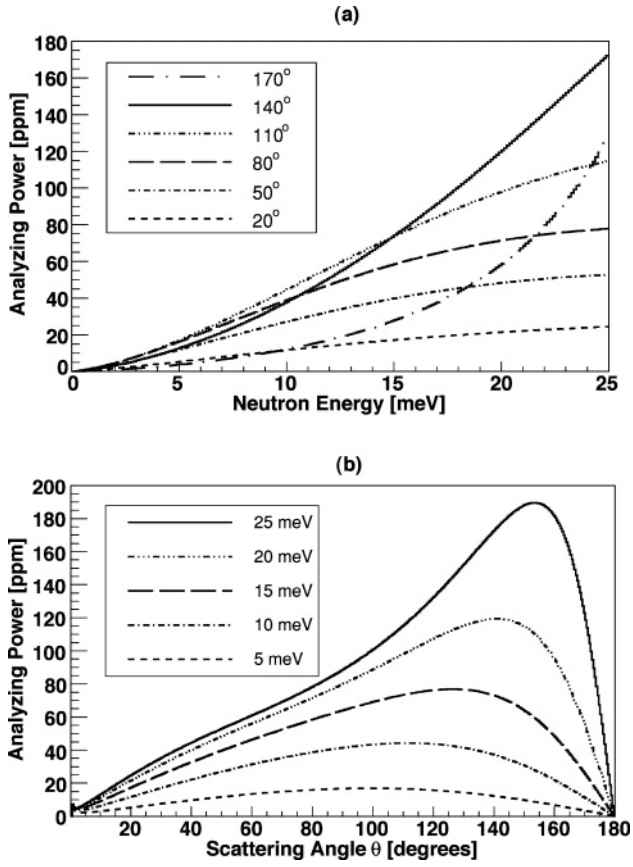

FIG. 15. Analyzing power for parahydrogen, with electron screening.

changes sign at small angles ($\theta \lesssim 1^\circ$) for all energies over which it was calculated in Figs. 14 and 15.

V. DISCUSSION

If an experimental observable depends on both the neutron polarization direction as well as the relative position of the neutron or the uniformity of neutron positions in a volume with respect to polarization then the Mott-Schwinger-induced beam steering may become a systematic effect that must be taken into account. This is especially true for high-precision measurements and observables that are very small.

Our results show that the Mott-Schwinger analyzing power is generally small at the low energies treated here, mostly producing *ppm*-level asymmetries in the number of transversely scattered neutrons, with respect to the neutron polarization. The exceptions are ^{3}He and ^{10}B, due to their large capture cross sections. The evaluation of ($J \neq 0$) targets is not strictly valid using the current formalism, but we assert that the results obtained for these targets still provide a good estimate at these low energies.

Our calculations of the analyzing power of a "bare" proton, the calculation first done by Schwinger [12], and the hydrogen atom (Figs. 2 and 3), show that electron screening has a large effect on the predicted size of the asymmetry as well as its energy and angular dependence. The results for parahydrogen predict an asymmetry that is two orders of magnitude larger than it is for the hydrogen atom by itself but comparable to the asymmetry for the unscreened proton.

Experimentally, the scattered neutrons are not always detected directly. It is very often the case that only secondary particles are detected, either directly from neutron decay or from decaying nuclei after neutron induced excitation. In this case the resulting expected asymmetry must be calculated from an integral over all scattering angles, weighted by a solid angle that depends on the particular detector geometry. In such cases, the systematic effects from Mott-Schwinger scattering could be either significantly enhanced or reduced, depending on the detector geometry.

ACKNOWLEDGMENTS

This work was supported in part by the U.S. Department of Energy (Office of Energy Research, under Contract W-7405-ENG-36), the National Science Foundation (Grant No. PHY-0100348), and the Natural Sciences and Engineering Research Council of Canada.

[1] M. J. Ramsey-Musolf, S. A. Page, Annu. Rev. Nucl. Part. Sci. **56**, 1 (2006).
[2] J. Erler and M. J. Ramsey-Musolf, Prog. Part. Nucl. Phys. **54**, 351 (2005).
[3] W. M. Snow, J. Res. Natl. Inst. Stand. Technol. **110**, 189 (2005).
[4] C. R. Gould, G. L. Greene, F. Plasil, and W. M. Snow, eds., *Fundamental Physics with Pulsed Neutron Beams* (World Scientific, Singapore, 2001).
[5] S. A. Page *et al*., J. Res. Natl. Inst. Stand. Technol. **110**, 195 (2005).
[6] A. Komives *et al*., J. Res. Natl. Inst. Stand. Technol. **110**, 221 (2005).
[7] J. D. Bowman *et al*., Measurement of the parity-violating gamma asymmetry A_γ in the capture of polarized cold neutrons by parahydrogen, $\vec{n} + p \rightarrow d + \gamma$, Tech. Rep. LA-UR-99-5432, Los Alamos National Laboratory (1999).
[8] W. M. Snow *et al*., Nucl. Instrum. Methods A **440**, 729 (2000).
[9] W. M. Snow *et al*., Nucl. Instrum. Methods A **515**, 563 (2003).
[10] G. S. Mitchell *et al*., Nucl. Instrum. Methods A **521**, 468 (2004).
[11] M. T. Gericke *et al*., Phys. Rev. C **74**, 065503 (2006).
[12] J. Schwinger, Phys. Rev. **73**, 407 (1948).
[13] C. G. Shull, Phys. Rev. Lett. **10**, 297 (1963).
[14] G. Obermair, Z. Phys. D **204**, 215 (1967).
[15] S. W. Lovesey, J. Phys. C **2**, 981 (1969).
[16] W. S. Hogan and R. G. Seyler , Phys. Rev. **177**, 1706 (1969).
[17] N. Alexander and K. Amos, Aust. J. Phys. **49**, 633 (1996).
[18] V. F. Sears, Phys. Rep. **141**, 281 (1986).
[19] E. Merzbacher, *Quantum Mechanics* (Wiley, New York, 1961).
[20] H. A. Bethe and R. Jackiw, *Intermediate Quantum Mechanics* (W. A. Benjamin, New York, 1968).
[21] S. DeBenedetti, *Nuclear Interactions* (Wiley, New York, 1966).
[22] M. Celli *et al*., J. Phys. Condens. Matter **11**, 10229 (1999).
[23] Data from Neutron News, Vol. 3, No. 3, (1992) 29-37 (http://www.ncnr.nist.gov/resources/n-lengths/).
[24] J. Byrne, Neutrons, *Nuclei and Matter* (Institute of Physics, Bristol and Philadelphia, 1995).
[25] H. Kaiser *et al*., Z. Phys. A **291**, 231 (1979).
[26] L. Koester, K. Knopf, and W. Waschkowski, Z. Phys. A **312**, 81 (1983).
[27] I. S. Gradshteyn and I. M. Ryzhik, *Table of Integrals, Series, and Products* (Academic Press, San Diego, 1980).
[28] H. Margenau and G. M. Murphey, *The Mathematics of Physics and Chemistry* (Van Nostrand Reinhold, New York, 1957).
[29] L. Pauling and E. B. Wilson, *Introduction to Quantum Mechanics* (McGraw-Hill, New York, 1935), p. 344.